Accepted Manuscript

Experimental and theoretical investigation effect of flavonols antioxidants on DNA damage

Ali A. Ensafi, E. Heydari-Soureshjani, M. Jafari-Asl, B. Rezaei, Jahan B. Ghasemi, Elham Aghaee

PII: S0003-2670(15)00811-9

DOI: 10.1016/j.aca.2015.06.014

Reference: ACA 233975

To appear in: *Analytica Chimica Acta*

Received Date: 10 April 2015

Revised Date: 30 May 2015

Accepted Date: 2 June 2015

Please cite this article as: A.A. Ensafi, E. Heydari-Soureshjani, M. Jafari-Asl, B. Rezaei, J.B. Ghasemi, E. Aghaee, Experimental and theoretical investigation effect of flavonols antioxidants on DNA damage, *Analytica Chimica Acta* (2015), doi: 10.1016/j.aca.2015.06.014.

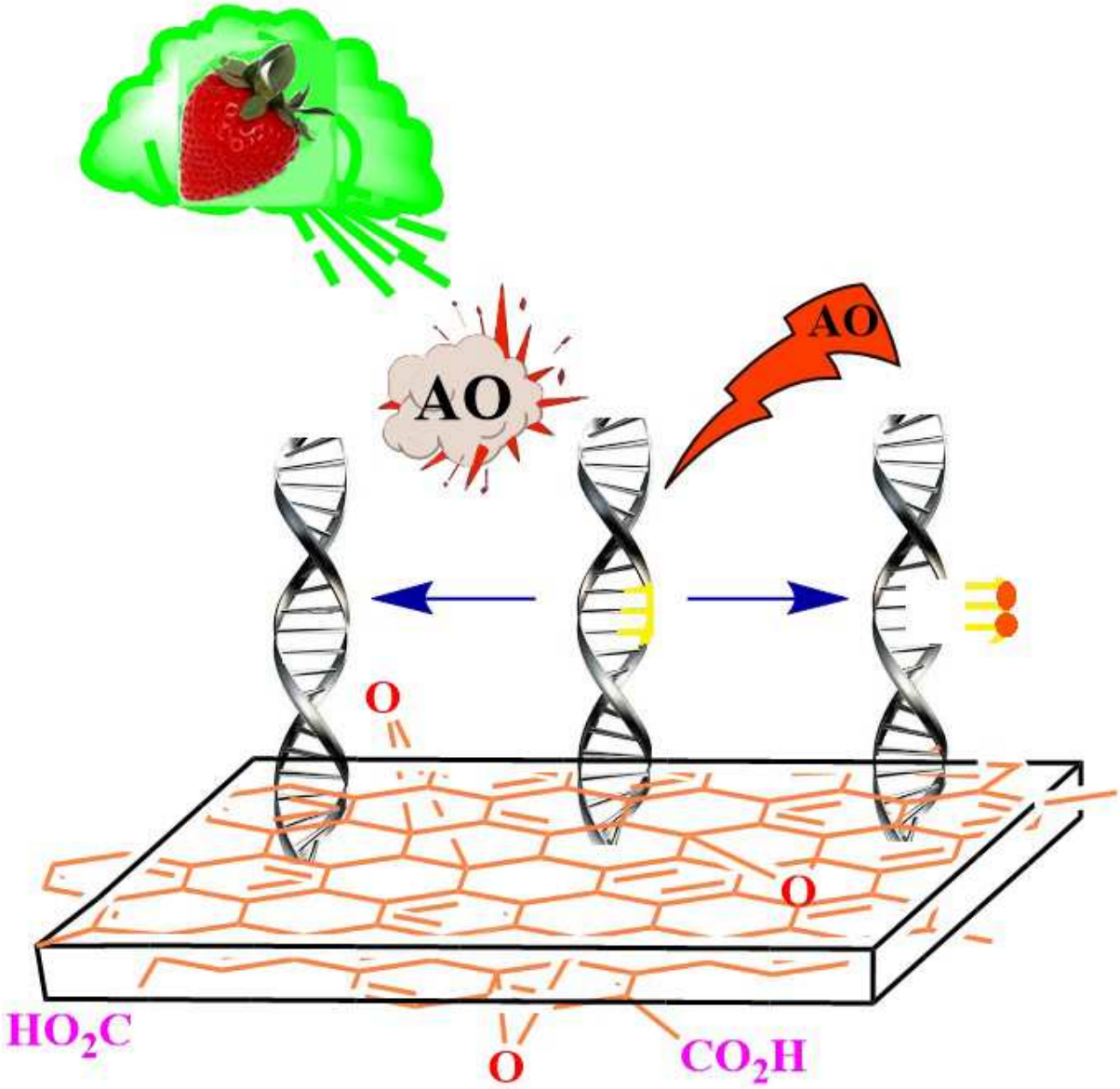

Experimental and theoretical investigation effect of flavonols antioxidants on DNA damage

Ali A. Ensafi[*1], E. Heydari-Soureshjani[1], M. Jafari-Asl[1], B. Rezaei[1], Jahan B. Ghasemi[2], Elham Aghaee[2]

(1) Department of Analytical Chemistry, Faculty of Chemistry, Isfahan University of Technology, Isfahan 84156–83111, Iran

(2) Drug Design in Silico Lab., Chemistry Faculty, K N Toosi University of Technology, Tehran, Iran

Abstract:

A new electrochemical biosensor was developed to demonstrate the effect of Acridine Orange (AO) on DNA damage. Then, the biosensor was used to check the inhibitors effect of three flavonols antioxidants (myricetin, fisetin and kaempferol) on DNA damage. Acridine Orange (AO) was used as a damaging agent because it shows a high affinity to nucleic acid and stretch of the double helical structure of DNA. Decreasing on the oxidation signals of adenine and guanine (in the DNA) in the presence of AO were used as probes to study the antioxidants power, using DNA-modified screen printed graphene electrode (DNA/SPGE). The results of our study showed that the DNA-biosensor could be suitable biosensor to investigate the inhibitors ability of the flavonols antioxidants on the DNA damage. The linear dependency was detected in the two regions in the ranges of 1.0 – 15.0 and 15.0 – 500.0 pmol L^{-1}. The detection limit were found 0.5 pmol L^{-1} and 0.6 pmol L^{-1} for guanine and adenine, respectively. To confirm the electrochemical results, Uv-Vis and fluorescence spectroscopic methods were used too. Finally molecular dynamic (MD) simulation was performed on the

* Corresponding Author: Phone: (98) 31–33913269. Fax: (98) 31–33912350. E–mail: Ensafi@cc.iut.ac.ir; aaensafi@gmail.com; ensafi@yahoo.com.

structure of DNA in a water box to study any interaction between the antioxidant, AO and DNA.

Keywords: Flavonols anti-oxidants; DNA damage; Graphene modified screen printed electrode; Voltammetry; Molecular docking.

1. Introduction

Flavonols are a class of flavonoids those are diverse groups of naturally occurring polyphenolic compounds ubiquitously distributed throughout the plane kingdom. The function of flavonoids in plants is controversial and poorly understood. Over the years bewildering arrays of biological effects have been ascribed to the flavonoids. These include but are not limited to antibacterial, antiviral and antifungal effects; anti-inflammatory and anti-angiogenic effects; anti-mutagenic, mutagenic, anti-proliferative, anti-cancer and anti-aging effects [1,2]. Similarly, recent epidemiological and experimental studies indicate that flavonols can also act as important proteasome inhibitors and apoptosis inductors [3]. In many countries, onions, apples, tea and red wine are the main dietary sources of flavonoids, also these are common in vegetable, fruits, plant and herbal medicines [4].

DNA is an important functional biomolecule, which has received considerable attention by researchers [5]. The detection of DNA damage has become one of the most important themes in DNA research fields because of the crucial role of DNA in mutagenesis, carcinogenesis and aging [6]. If the damaged DNA cannot be repaired properly, the caused gene mutation will result in cancer and tumor in DNA replication process [7,8]. Thus, quick, economical and sensitive screening of new chemicals in vitro for potential toxicity and before their exposure to environment in commercial use is of great significance.

While 32P–postlabelling, chromatographic or electrophoretic separation of hydrolyzed samples have been coupled with mass spectrometry [9], fluorescence, and photoelectrochemical [10] may provide detailed molecular information on DNA damage. Microbiological and animal toxicity tests may suggest some direct proof for genotoxicity [11]. All of the methods are exhausting or wasting much time and may include costly instruments. In contrast, electrochemical methods are fast, simple and selective tools to provide detailed molecular information on DNA damage **[**12-14]. The DNA electrochemical biosensor is a device that incorporates immobilized DNA as the molecular identification element in the biologically active layer on the electrode surface, and measures specific binding processes with DNA using an electrochemical transducer. The electrochemical DNA–biosensor has been used to sense in situ oxidative damage to DNA. The electrochemical data can contribute to the explanation of the mechanism by which DNA is oxidized by some compounds with a view to what happen in the living cell [15,16]. Interactions of various substances with ds-DNA have been studied using DNA–electrochemical [17,18], and permit explanation of the interaction with ds-DNA as well as its electrochemical mechanism.

Acridine orange (AO) is a nitrogen-containing aromatic dye with a basic structure of 3,6-bis(dimethylamino)-acridine monohydrochloride, whose planar structure is come from anthracene [19]. It shows a high attraction for nucleic acid and intercalates into double strain DNA (ds-DNA) or binds electrostatically to single strain DNA (ss-DNA). This compound can further oxidative damage to DNA in cancerous cells through the generation of reactive oxygen species [20]. AO bind DNA via intercalative manner and slip between next base pairs and stabilizes pigment–DNA complexes through charge neutralization of DNA backbone phosphate group [21], which cause stretch of double helical structure [22-24]. Moreover, the

stacking contacts are formed between ligand molecules and DNA base pairs while the lengthening of DNA occur cause untwisting of helix [25,26].

In this work, AO was used as a model for DNA damage because it can intercalates into ds-DNA or binds electrostatically to ss-DNA and slip between adjacent base pairs and cause stretch of double helical structure. Reduced graphing oxide (rGO) was used at the surface of screen printed carbon electrode. Then, DNA-modified screen printed graphene electrode (DNA/SPGE), was prepared. Then, decreasing on the oxidation signals of adenine and guanine (in the DNA) in the presence of AO were used as probes to study the antioxidants power. The effect of three flavonols antioxidants (myricetin, fisetin and kaempferol) to inhibit the degradation of ds-DNA were studied using electrochemical and spectroscopic methods. In the second section of this study, molecular docking was used to investigate the interaction of DNA/AO and DNA/flavonols. The theoretical results confirm the experimental observations. The anti-damaging effects of kaempferol and fisetin are comparable with myricetin.

2. Experimental

2.1. Chemicals and materials

All chemicals were of reagent grade quality and used as received without further purification. Graphite, nitric acid and hydrofluoric acid were purchased from Merck. AO, double-stranded salmon sperm DNA (ds-DNA, catalog No. D8899), reagent grade Tris–HCl, CH_3COOH, NaCl and NaOH were purchased from Aldrich Chemicals (Milwaukee, USA). A salmon sperm ds-DNA stock solution (100 mg L^{-1}) was prepared in Tris–HCl buffer and kept frozen. More diluted solutions of the ds-DNA were prepared with acetate buffer solution (pH 4.8) containing 0.02 mol L^{-1} NaCl. 1.0 mmol L^{-1} AO solution was prepared too.

2.2. Apparatus

Field emission scanning electron microscopy (FE–SEM) was made on a Philips XL–30 ESEM at an accelerating voltage of 20 kV. Fourier transform–IR spectra were recorded using a JASCO FT–IR (680 plus) spectrometer, the vibrational transition frequencies are reported in wavenumbers (cm^{-1}). The fluorescence signal was measured using a Jasco FP750 spectrofluorometer with an excitation radiation at 485 nm. UV–Vis spectra were measured with a double beam spectrophotometer, Jasco model V–750 using 1.0 cm quartz cells.

A µ-Autolab electrochemical analyzer, Model PGSTAT 302N potentiostat/ galvanostat (Eco–Chemie, the Netherlands), controlled by a microcomputer was used for all voltammetric and Autolab electrochemical analyzer, Model PGSTAT30 potentiostat/galvanostat (Eco–Chemie, the Netherlands), was used for electrochemical impedance spectroscopy study. Data were acquired and processed using GPSE computrace software 4.9.007. A standard three-electrode cell contained a platinum wire auxiliary electrode, a saturated Ag/AgCl reference electrode (KCl sat'd) and the screen printed graphite electrode (SPGE) was used in all the experiments. All the electroanalytical measurements were performed at room temperature.

Molecular docking is an attractive study to understand ligand-receptor interactions. The DNA sequence $d(ACCGACGTCGGT)_2$ was taken from the Protein Data Bank (PDB id: 423D) at a resolution of 1.60˚A. (http://www.pdb.org). Several conformers of DNA were taken from the MD simulation and subjected to docking for representing conformational changes and flexibility of DNA. Binding sites were identified from the cavities within the structure of DNA duplex with Discovery Studio 2.5 [27] (Accelrys Inc, San Diego, CA, USA). For preparation step of DNA, CHARMm force field was applied, hydrogen atoms were added and all water molecules were removed.

Molecular docking simulations were carried out with Discovery Studio 2.5. GOLD program was used to dock antioxidants into the DNA duplex [28]. GOLD is a genetic algorithm for the docking of flexible ligands into receptor binding sites which accounts the side chain flexibility for the target receptor. The chemical structure of the antioxidants were constructed by Hyperchem package (Ver. 7.0), and energy minimizations were performed by AM1 semi-empirical method with Polak–Ribiere algorithm (root mean square gradient of 0.01 kcal mol^{-1}). The resulting structures were imported into Discovery Studio, and typed with CHARMm force field and partial charges were calculated by Momany-Rone option [29]. Then, they were minimized with Smart Minimize, which performs 1000 steps of steepest descent with a RMS gradient tolerance of 3, followed by conjugate gradient minimization. Other parameters were set as the default protocol settings. Finally, Gold score was used to evaluate the affinity of antioxidants toward the candidate pocket of HSA.

Molecular dynamic (MD) simulation was performed on the structure of DNA in a water box. The MD simulations were performed with the GROMACS 4.5.3 simulation package [30] by the use of Amber99 force field [31]. Then the system was placed in cubic box (7.54×7.54×7.54 nm3). Water molecules were added using a simple charge (SPC216) model [32] and the solvated system was neutralized by adding twenty two sodium ions in the simulation. An energy minimization step was performed for the full system without constraints using the steepest descent integrator for 50000 steps, until a tolerance of 10 kJ mol^{-1}. This was followed by a short (200 ps) position restrained equilibration simulation at 310 K. Finally, molecular dynamics simulations were performed for a period of 5 ns with a time step of 2 fs. The LINCS algorithm (Linear Constraint Solver) which is three to four times faster than the SHAKE algorithm was used to constrain the length of covalent bonds [33]. The Particle–Mesh Ewald (PME) summation technique was used to compute long-ranged electrostatic interactions [34,35]. The Coulomb and van der Waal's cut-offs were set

to 1.0 and 1.4 nm, respectively. The constant temperature and pressure (NPT) ensemble at 310K with periodic boundary conditions was used to perform the simulation. Initial velocities were assigned from Maxwell distribution at 310 K. The Berendsen thermostat was applied to keep the temperature constant [36]. The stability of system and the structural geometry was examined by mean of the deviation (RMSD) of DNA with respect to initial structure of DNA. The average RMSD value of DNA backbone was calculated to be 5.50 nm. The average structures of DNA were calculated for the time intervals: 1000-2000, 2000-3000, … , 4000-5000 ps and were used for docking.

2.3. Synthesis of exfoliated graphene oxide

Graphene oxide was prepared using a modified Staudenmaier method [37]. Natural graphite powder (with a particle size of 70 µm and a purity of 99.999%) was chemically oxidized form graphite oxide (GO) at room temperature. Graphite (1.0 g) was continuously stirred in a mixed solution of conc. sulfuric acid (20 mL), conc. nitric acid (10 mL) and potassium chlorate (10.0 g) for approximately 100 h. The resulting GO was rinsed with 5.0 wt% (w/w) HCl aqueous solution and then repeatedly washed with deionized water until the pH of the filtrate became neutral and the product was dried in air [37].

2.4. Electrochemical deposition of graphene oxide on the screen printed carbon electrode

Pretreatment of screen printed carbon electrode (SPCE) was carried out before electro-reduction of graphene oxide, to create porosity on the surface of SPCE by removing impurities for the immobilization .The reason for the low activity may result from the lack of functional groups on the surface [38]. Electrochemical deposition was carried out in a

deaerated borate buffer solution (pH 9.0) containing 0.5 mg mL^{-1} GO with running cyclic voltammogram (CV) with stirring, for ten cycles from 0.60 to –1.60 V at scan rate 25 mV s^{-1}.

2.5. Preparation of DNA–biosensor and procedure

For adsorptive of the ds-DNA on a SPGE, the ds-DNA was immobilized on a SPGE surface by applying a potential at +0.45 V for different preselected times (optimum time of 180 s) from a stirred (constant rate) solution containing 20.0 mg L^{-1} ds-DNA in the acetate buffer containing 0.02 mol L^{-1} NaCl. The electrode was then gently rinsed with the acetate buffer to remove unbounded ds-DNA. The voltammetric stripping step was performed by employing a positive-going differential pulse potential scan (from 0.40 to 1.40), using a pulse amplitude of 0.06 V, a modulation time of 0.04 s and a step potential of 0.01 V in the acetate buffer plus 0.02 mol L^{-1} NaCl to have the blank signals of the biosensor. The oxidation signals of guanine and adenine were recorded. The procedure was repeated using a new modified-SPGE in a phosphate buffer solution (pH 7.0) containing different concentrations of AO when the solution was stirred at constant rate for 120 s at open circuit. After accumulation of AO, the ds-DNA–modified SPGE was rinsed. Then, differential pulse voltammograms in the blank solution (the acetate buffer plus 0.02 mol L^{-1} NaCl) were recorded to have the biosensor-AO signals.

In order to investigate the effect of three kinds of antioxidant (kaempferol, myricetin and fisetin) to the distractive effect of AO on the ds-DNA, the DNA biosensor immersed into a phosphate buffer solution (pH 7.0) containing different concentrations of AO and constant concentration of the antioxidant (1.0×10^{-1}¸1.0×10^{-3} and 1.0×10^{-5} µmol L^{-1}) when the solution was stirred at constant rate for 120 s at an open circuit system. After accumulation of AO and the antioxidant, the ds-DNA–modified SPGE was rinsed. Then, the differential pulse voltammogram was recorded in the blank solution (the acetate buffer plus 0.02 mol L^{-1}

NaCl). The raw data were treated using the Savitzky and Golay filter (level 2) of the GPES software, followed by the GPES software moving average baseline correction, using a "peak width" of 0.02 (this method in all experiment was used).

2.6. Uv–Vis and fluorescent study

UV–Vis spectra of the blank solution (containing Tris–HCl buffer (pH 7.0) and acetate buffer solution (pH 4.8) containing 0.02 mol L^{-1} NaCl), ds-DNA (30 mgL^{-1}), AO (20.0 µmol L^{-1}) and ds-DNA in the presence of AO at concentration of (20.0 µmol L^{-1}) were recorded in the wavelength of 200 to 600 nm. The graph was constructed as the absorbance *vs.* wavelength.

The fluorescence signal of different concentrations of AO in the presence of ds-DNA (20 mg L^{-1}) was recorded. Then, the effects of three kinds of antioxidant (kaempferol, myricetin and fisetin) to the distractive effect of AO on the ds-DNA were investigated using three concentrations of the antioxidant (0.01¸1.0 and 100 nmol L^{-1}) in the presence of different concentrations of AO. The graph was constructed as the fluorescent signal *vs.* wavelength. Then, the fluorescence signal of each concentration of AO at 524 nm was selected and the graph was constructed as the fluorescence signal *vs.* the AO concentration, then the slope of all graphs were reviewed.

3. Results and discussion

3.1. Characterization of the screen printed graphene electrode

Electrochemical methods were used to characterize the SPGE. Fig. 1a shows a typical CVs of the ten successive scan for the electrochemical reduction of EGO at pH 9.0 (borate buffer). This reveals that the graphite oxide (GO) was wholly exfoliated as individual GO sheets at pH 9.0 with ultrasonication. It is broadly accepted that the peak at ca. −1.40 V is attributed to

the irreversible electrochemical reduction of exfoliated graphene oxide (EGO) [38,39]. The continuous increasing in the peak current with successive CV scans (Fig. 1 a) indicated that EGO was successfully reduced to rGO, and attached onto the electrode surface. Despite EGO can form well dispersed aqueous colloids; it is well known that electrochemical reduction of EGO sheets in aqueous solutions results in their irreversible agglomerate. Therefore, it is reasonable to speculate that when EGO sheets in direct contact with an electrode surface, it electrochemically was reduced. The resulted graphene sheets will also be insoluble, and thus directly attach to the electrode surface [39,40].

$Fe(CN)_6^{3-/4-}$, as a redox probe, was used to evaluate the screen printed carbon electrode (SPCE) and SPGE (Fig. 1b). The modified SPGE showed a slightly smaller peak potential separation and larger peak current than the SPCE. The improved performance demonstrated faster electron transfer and larger electroactive surface area of the electrochemically rGO-modified electrode. These results also indicated that the ferrocyanide electrochemistry at the SPGE and SPCE mainly took place within a 3D porous electrode structure.

AC impedance spectroscopy was also used to evaluate the SPCE and SPGE. Fig. 1c shows the Nyquist diagrams of the electron transfer kinetic for the redox probe at the SPCE and SPGE, in 0.10 mmol L^{-1} $[Fe(CN)_6]^{3-/4-}$. It can be seen that a small and well defined semi-circle obtained at the SPCE at higher frequencies, indicating small interface impedance. However, the electron resistance of SPCE decreased remarkably after electrochemical deposition of EGO on the surface of SPCE, suggesting the excellent electro-conductivity of SPGE. **"Here Fig. 1"**

FT–IR (Fig. 2a) and Raman (Fig. 2b) spectroscopy were used to examine the reduction degree of rGO. The FT–IR spectrum of EGO presented the characteristic absorption bands corresponding to the stretching of O–H, C=O of carboxyl and carbonyl groups, C=C, C–O–C and C–O. After the electrochemical reduction of GO, most of the absorption bands

disappeared, only the peak of C=C (1618 cm^{-1}) and a weak peak of C=O (1741 cm^{-1}) remained, which proved the effective elimination of the oxygen-containing groups. The Raman spectrum of EGO contained both G and D bands at 1355 and 1595 cm^{-1}, respectively. The Raman spectrum and the ratio of bond D to bond G shown the reduction degree of the graphene oxide to reduce graphene oxide. FE–SEM images of SPCE and SPGE showed a typical wrinkled sheet texture of graphene too as shown in Fig. 2c and Fig. 2d, respectively. EDX was also used to confirm the reduction of graphene oxide. The results confirmed that after reduction of graphene oxide the oxygen percentage reduces from 47.37% to 36.38%. This is due to the reduction of oxygenated functional groups at the surface of the graphene oxide. The results are shown in Figs. 2E, 2F and are given in Table 1 [41,42].

"Here Fig. 2 and Table 1"

3.2. Electrochemical optimization

To camper SPCE and SPGE as a substrate for immobilizing of the DNA, differential pulse voltammograms of ds-DNA at the surfaces of these two electrodes were recorded. The result showed that the oxidation peaks current of guanine and adenine at the DNA/SPGE is higher than the DNA/SPCE because the surface area of modified electrode was increased and more DNA can adsorb on the surface of the SPGE. (Fig. S-1)

To get the maximum sensitivity, the influence of experimental parameters affect the fabrication of the biosensor, including adsorption potential of the dsDNA at SPGE, concentration and accumulation time of the DNA in preparing DNA-SPGE were studied. The oxidation signals of guanine and adenine at the DNA–biosensor, before and after interaction with AO on the electrode surface, were used as probes using differential pulse voltammetry (DPV). To find the optimum adsorption potential of DNA, six different potential (between 0.00 and +0.60 V) were selected. The results of our studied showed that the DPV signals increased till +0.45 V and then levelled off, as shown in Fig. 3A. To find the optimum

concentration of the ds-DNA, five different concentrations of the ds-DNA (between 5.0 and 35.0 mg L^{-1}) were tested. The results of our studied (Fig. 3B) showed that the guanine and adenine signals at the electrode surface were increased by increasing the DNA concentration up to 20.0 mg L^{-1}, and then levelled off. Therefore, 20.0 mg L^{-1} of salmon sperm ds-DNA was selected to fabricate the biosensor. To find the optimum accumulation time for the ds-DNA at the surface of SPGE, five different times (between 60 and 360 s) were selected using 20.0 mg L^{-1} ds-DNA at 0.45 V. The DPV signals of the guanine and adenine increased till 180 s and then levelled off (Fig. 3C). Therefore, 180 s was considered as an optimum accumulation time.

The binding of AO with the ds-DNA at the DNA-biosensor depends on the interaction (incubation) time too. The incubation time for the interaction of AO with the DNA–biosensor was optimized during 60-240 s. The results (Fig. 3D) showed that by increasing the incubation time up to 120 s, the oxidation peaks current of adenine and guanine decreased till 120 s and then they were levelled off for the longer incubation time. Accordingly, 120 s was selected as the optimum time for the interaction of AO with the DNA–biosensor.

"Here Fig. 3"

The effect of solution pH on the interaction of AO with the DNA-SPGE was also investigated in 0.10 mol L^{-1} PBS at different pH levels (in the range of 2.0–10.0) containing 1.0×10^{-2} µmol L^{-1} AO with stirring. The variations on the peaks potential and peaks current of the adenine and guanine were recorded at different pH, using DPV. The optimum pH of the measurement was found to be 7.0.

After adsorption of the DNA on the surface of electrode, we couldn't use the electrode more than one measurement and therefore, they had to be replaced each time. The reproducibility results (RSD%) (n=5) of the measuring of adenine and guanine peaks current (after accumulation of the dsDNA on the surface SPGE) was calculated as 7.4%.

3.3. Interaction of AO with the ds-DNA

The oxidation signals of the guanine and adenine at DNA–biosensor, before and after interaction with AO, are shown in Fig. 4A. Different concentrations of AO were used to interact with the ds-DNA on the surface of the DNA–biosensor. The results showed that the oxidation signals of guanine and adenine obtained with the ds-DNA–modified electrode before interaction of AO were higher than the one obtained after interaction with AO. Decreasing of the oxidation signals of guanine and adenine bases were attributed to the binding of AO to these electroactive DNA bases. This decreasing could be explained as a possible damage or shielding of the oxidizable groups of guanine and adenine bases while AO interacts with the ds-DNA either on SPGE surface. The percentage of reduction on the oxidation peaks current of guanine and adenine were 54.82% and 54.90%, respectively. These type of experiments are very important to determine DNA sites and rational design of new DNA–targeted molecules for the applications in cancer therapy. Our obtained results showed that DNA–biosensor might be used for the detection of AO interaction with the ds-DNA. Using DPV and following the changes in the oxidation signals intensity of guanine and adenine, after their interactions with AO, the linear dependency was detected in the two concentration ranges of 1.0 – 15.0 and 15.0 – 500.0 pmol L^{-1}. The regression equations for guanine were $I(\mu A) = 0.1446C_{AO} + 0.4572$ with $R^2 = 0.9943$ and $I(\mu A) = 0.0017C_{AO} + 2.5391$ with $R^2 = 0.9989$, respectively and for adenine were $I(\mu A) = 0.1405C_{AO} + 0.6567$ with $R^2 = 0.9845$ and $I(\mu A) = 0.0032C_{AO} + 3.0814$ with $R^2 = 0.9852$ where C is the concentration of AO in pmol L^{-1}. The detection limit (3Sb/m, four times of the standard deviation of the blank divided by the slope of the calibration curve) were found 0.5 pmol L^{-1} and 0.6 pmol L^{-1} for guanine and adenine, respectively. **"Here Fig. 4"**

3.4. Inhibition effect of the antioxidants on the interaction between ds-DNA and AO

DPV oxidation signals of guanine and adenine at DNA–biosensor, before and after interaction with AO in the present of the three kinds of the antioxidants, on the electrode surface, are shown in Fig. 4 (B: fisetin, C: kaempferol and D: myricetin). Different concentrations of AO along constant concentration of each of the antioxidants were used to interact with the ds-DNA on the surface of the DNA–biosensor. The results showed that the oxidation signals of guanine and adenine remained nearly constant after interaction of AO with the ds-DNA at the electrode surface in the present of each of the antioxidants. The percentage of the decreasing in the oxidation peaks current of guanine and adenine were 3.59% and 6.06%, 10.89% and 10.57%, 26.7% and 17.55%, for in the presence of kaempferol, fisetin and myricetin, respectively. As described before, the percentage of the reduction on the oxidation peaks current of guanine and adenine in the absence of these antioxidants were 54.82% and 54.90%, respectively. These results confirm that the antioxidants inhibited the DNA damage by AO. The results of our studied also confirm that the anti-damaging effects of kaempferol and fisetin are comparable with myricetin.

To emphasize the electrochemical method, fluorescence signal of AO in the presence of DNA was recorded with and without of the antioxidants (myricetin, fisetin and kaempferol). It is clear that the fluorescence intensity of AO in the presence of myricetin, fisetin and/or kaempferol was different *vs.* its fluorescence signal in the absence of the antioxidants. The results of this study revealed the anti-damaging effect of these antioxidants in the interaction of AO with dsDNA. In order to evaluate the endurable inhabit effect of the antioxidants, the fluorescence signal of AO was recorded with different concentration of AO in the presence of different concentrations of myricetin, fisetin and kaempferol (to draw the calibration curves of AO). Fig. 5 shows the fluorescence spectra and the linear variations in the fluorescence intensities of AO vs. its concentration in the presence of the ds-DNA (20.0 mg L^{-1}) and 0.01 nmol L^{-1} from A: fisetin, B: kaempferol and C: myricetin. The same results for the other

concentrations of the antioxidants are given in Table 2 and Figs. S-2, S-3 and S-4. The results showed that the AO fluorescence intensity (in the presence of the ds-DNA) was significantly changed in the presence of myricetin, fisetin and/or kaempferol. The results in Table 2 confirms that lower concentration of the antioxidants (*vs.* AO) are enough to prevent the DNA damage. The binding of AO to ds-DNA extremely causes increasing in the fluorescence intensity so the slope of the calibration curve increases, whereas in the presence of the antioxidants the intercalation of AO to ds-DNA was reduced and therefore the slope of the fluorescence calibration curve was decreased. The possibility of the fluorescence intensity being affected by a quenching effect caused by weak interactions of the dye with antioxidant molecules are also studied in the presence of 25 nmol L^{-1} AO in the presence of 1.0 µmol L^{-1} myricetin, or fisetin and/or kaempferol. The results (Fig. 6, A: AO, B: kaempferol, C: fisetin and D myricetin) confirmed that the antioxidants did not have any interaction with AO to can quench the fluorescence signal. The results confirmed the anti-damaging effects of kaempferol and fisetin are comparable with myricetin, which are consistent with the DPV results.

"Here Fig. 5, Fig. 6 and Table 2"

3.5. Calculation of association constant of AO with DNA

According to the method of Qu et al. [43] it is assumed that DNA and AO only produced a single complex $DNA.AO_m$ according to the following reaction:

$$DNA + mAO \leftrightarrow DNA.AO_m \quad (1)$$

The peak current (of the DP voltammogram) is most sensitive to the equilibrium constant of $DNA.AO_m$ complex. The decreasing the peak current is proportional to the concentration of $DNA.AO_m$ complex. In terms of the all-or-none (Hill) cooperative of multiple ligand binding [44,45], the fraction of DNA to which AO is bound as $DNA.AO_m$, relative to the total DNA concentration in the supporting electrolyte $[DNA]_0 = [DNA.AO_m]_{max}$ is given by:

$f = [DNA.AO_m]/[DNA.AO_m]_{max} = [AO]^m/([AO]^m + K_d^m])$ and $K_d^m = [AO]^m(1-f)/f$ (2)

where $[DNA.AO_m]_{max}$ is the maximum concentration of the complexed binding sites, [AO] is the concentration of free AO, K_d is the dissociation equilibrium constant and m is the Hill coefficient. Note that $K_d = [AO]_{0.5}$, i.e., at half occupation. The association constant K_a is given by the reciprocity: $K_a = K_d^{-1}$. It is not advisable to use the overall constant $K = (K_a)^m$, which would have the physically meaningless dimension of M^{-m}. The interaction partners for AO is the binding sites of DNA. Mass conservation dictates that:

$$[DNA] = [DNA.AO_m]_{max} - [DNA.AO_m] \quad (3)$$

$$[AO] = [AO]_0 - [DNA.AO_m] \quad (4)$$

where $[AO]_0$ is the total concentration of AO. According to the Ilkovic equation for an irreversible electrode [46].

$$I = k.[AO] \quad (5)$$

where k is a constant. According to the above equation, the current difference ΔI is defined as: and that Insertion of Eqs. (3) and (4) into Eq. (5) yields

$$\Delta I = k([AO]_0 - [AO]) = k.m.[DNA.AO_m] \quad (6)$$

From Eq. (2), we obtain that:

$$\log[f/(1-f)] = m.\log (K_a/M^{-1}) + m.(\log[AO]/M). \quad (7)$$

$$\text{and } \mathrm{Log}[\Delta I/(\Delta I_{max} - \Delta I)] = m(\log K_a/M^{-1}) + m.\log ([AO]/M). \quad (8)$$

By keeping the DNA concentration at 20 mg L^{-1} and varying the concentration of AO, a plot of $\log[\Delta I/(\Delta I_{max} - \Delta I)]$ as a function of log([AO]/M) is a linear with a slope of m. From the results, m = 0.46 and $K_a = 8.2 \times 10^9$ M^{-1} were obtained in the concentration range of the applied AO.

3.6. Molecular docking of AO and the antioxidants with the DNA sequenced $(ACCGACGTCGGT)_2$

Several conformers of DNA were taken from the MD simulation and subjected to docking for representing conformational changes and flexibility of DNA. The chemical structure of AO and the antioxidants were constructed by Hyperchem package (Ver. 7.0), and energy minimizations were performed by AM1 semi-empirical method with Polak–Ribiere algorithm (root mean square gradient of 0.01 kcal mol^{-1}). To provide a better representation of the system, an ensemble of DNA conformers and not a single structure was used. Docking against several structures of the DNA increases the chance of finding a receptor in the right conformational state to embed a given ligand. Therefore, the average structures of DNA were calculated for the time intervals: 1000-2000, 2000-3000, …, 4000-5000 ps.. It should be noted that not all of these conformations were able to interact with the given molecules. Binding sites were derived from the cavities within the structure of DNA duplex. Since different conformers of DNA has been used, three binding sites (a, b and c) were found on the average structures of DNA duplex at different time intervals and thus the given molecules can interact with the DNA in these three sites. For example, fisetin interacts with the three parts of DNA duplex as shown in Fig. 7. It can be seen that the hydroxyl group of fisetin can form two hydrogen bonds with nucleobase DG7 (in the site b) of the average structure of 1000-2000 ps, while there is no interaction between fisetin and DNA from 2000 to 3000 ps. Molecular docking of the average structure of 3000-4000 ps reveals that there are two hydrogen bonds between DG16 base and the hydroxyl group of fisetin and there is a hydrogen bond between DT12 and fisetin, while the aromatic ring of fisetin has two π-σ interactions with DG16 and DT12 (site a). There are also three hbonds between the nocleobases DG4 and DG23 of the average structure of 4000-5000 ps and fisetin (site a).

“Here Fig. 7”

Kaempferol interacts with the three binding sites of DNA duplex in the different time intervals. For example hydrogen bonding interaction was found between hydroxyl groups of

kaempferol and DG10 and DC15 base (site a) of the average structure of 3000-4000 ps, between hydroxyl groups of kaempferol and DT8, and the oxygen atom of kaempferol with the base DG16 (site a) of the average structure of 4000-5000 ps. There were other H-bond interactions between the average structure of 4000-5000 ps and kaempferol in the site c (the oxygen atom of kaempferol–hydrogen of DG4 and the nitrogen atom of DG23-hydrogen of kaempferol).

The resulting docking model revealed that myricetin can interact with the three binding sites of DNA duplex as well as fisetin and kaempferol. For example, there are three hydrogen bonds between hydroxyl group and two hydrogen atoms of myricetin and hydrogen, oxygen and amine groups of DG16 respectively, and a H-bond interaction between DT12 and myricetin, while the aromatic ring of myricetin has a π-σ interaction with DT12 (site a). The values of the GOLD score obtained are listed in Table 3. These GOLD score values indicate the high binding affinity between the ds-DNA and antioxidants.

The docking models revealed that there is a hydrogen bond between N15 atom of AO and DG16 base (3.29 Å). Also, there are hydrophobic contacts between C3 and C13 with DA17, between C5 and C6 with DG11, between C3 withDG16, between C20 with DC18, between C19 with DC9 and between C8 and DG10.The binding constant for interaction AO with DNA found to be 2.80×10^5 mol L^{-1}. **“Here Table 3”**

4. Conclusions

Damage to the genome of living cells is apparently a normal part of cell functioning. There is continuous and significant damage to the DNA from many sources, all of which can lead to mutations and chromosomal aberrations that compromise the fidelity and integrity of the genome. Repair of all types of DNA damage and also prevent DNA damage to be an important factor in healthy cells. In this paper an electrochemical biosensor was developed

(DNA/SPGE) to demonstrate the effect of AO on DNA damage. The reductions in the intensities of guanine and adenine oxidation signals after their interaction with AO were used as indicators in electrochemical study. Then, three kinds of flavonols antioxidants (myricetin, fisetin and kaempferol) were used as anti-damaging model. The inhibition of the DNA damage was investigated by electrochemical and fluorescence methods. Moreover, to confirm the experimental results, molecular docking as a theoretical method was used too. The obtained results showed that if the factor of inhibition of injuries to DNA, make weak interaction with DNA, it will be possible to use it as an anti-damaging drug, but if it make strong, it can damage to DNA itself. With consideration of the experimental and theoretical results, as much as constant binding is more, this effect is less and cannot inhibit the interaction of AO with DNA. The results shown the anti-damaging effects of kaempferol and fisetin is better than myricetin.

Acknowledgments

The authors wish to thank Iran National Science Foundation and National Elites Foundation for their support.

References

[1] R. Popp, O. Schimmer, Induction of sister-chromatid exchange (SCE), polyploidy, and micronuclei by plant flavonoids in human lymphocyte cultures. A comparative study of 19 flavonoids, Mutat Res. 246 (1991) 205–13.

[2] K. T. Howitz, K. J. Bitterman, H. Y. Cohen, D. W. Lamming, S. lavu, J. G. Wood, R. E. Zipkin, P. Chung, A. Kisielewski, L. Zhang, B. Scherer, D. A. Sinclair, Small molecule activators of sirtuins extend Saccharomyces cerevisiae lifespan, Nature 425 (2003) 191–196.

[3] D. Chen, K. G. Daniel, M. S. Chen, D. J. Kuhn, K. R. Landis-Piwowar, Q. P. Dou, Dietary flavonoids are proteasome inhibitors and apoptosis inducers in human leukemia cells, Biochem. Pharmacol. 69 (2005) 1421–1432.

[4] M. Zatloukalovà, V. Křen, R. Gažàk, M. Kubala, P. Trouillas, J. Ulrichovà, J. Vacek, Electrochemical investigation of flavonolignans and study of their interactions with DNA in the presence of Cu(II), Bioelectrochemistry 82 (2011) 117–124.

[5] A. A. Ensafi, M. Amini, B. Rezaei, Detection of DNA damage induced by chromium/glutathione/H2O2 system at MWCNTs–poly(diallyldimethylammonium chloride) modified pencil graphite electrode using methylene blue as an electroactive probe, Sens. Actuators B 177 (2013) 862– 870.

[6] D.O. Hull, B. Bajrami, I. Jansson, J.B. Schenkman, J.F. Rusling, Characterizing metabolic inhibition using electrochemical enzyme/DNA biosensors, Anal. Chem. 81 (2009) 716-724.

[7] Y. Liu, N. Hu, Electrochemical detection of natural DNA damage induced by ferritin/ascorbic acid/H_2O_2 system and amplification of DNA damage by endonuclease Fpg, Biosens. Bioelectron. 25 (2009) 185–190.

[8] G. Chiti, G. Marrazza, M. Mascini, Electrochemical DNA biosensor for environmental monitoring, Anal. Chim. Acta 427 (2001) 155–164.

[9] R. Kumar, P. Vodicka, K. Peltonen, K. Hemminki, 32P-postlabelling analysis of isomeric 7-alkylguanine adducts of styrene oxide, Carcinogenesis 18 (1997) 407–414.

[10] V. Viswesh, K. Gates, D. Sun, Characterization of DNA damage induced by a natural product antitumor antibiotic leinamycin in human cancer cells, Chem. Research in Toxicol. 23 (2010) 99–107.

[11] Y. Wang, H. Xiong, X. Zhang, S. Wang, Electrochemical biosensors for the detection of oxidative DNA damage induced by Fenton reagents in ionic liquid, Sensors and Actuators B 161 (2012) 274–278.

[12] A. A. Ensafi, B. Rezaei, M. Amini, E. Heydari-Bafrooei, A novel sensitive DNA–biosensor for detection of a carcinogen, Sudan II, using electrochemically treated pencil graphite electrode by voltammetric methods, Talanta 88 (2012) 244–251.

[13] J. Labuda, A.M. Oliveria Brett, G. Evtugyn, M. Fojta, M. Mascini, M. Ozsoz, I. Palchetti, E. Palecek, J. Wang, Electrochemical nucleic acid-based biosensors concepts, terms, and methodology (IUPAC Technical Report), Pure and Applied Chemistry 82 (2010) 1161–1187.

[14] R. N. Goyal, S. Bishnoi, Sensitive voltammetric sensor for the determination of oxidative DNA damage in calf thymus DNA, Biosens. Bioelectron. 26 (2010) 463–471.

[15] Y. Wang, H. Xiong, X. Zhang, S. Wang, Detection of rutin at DNA modified carbon paste electrode based on a mixture of ionic liquid and paraffin oil as a binder, Microchim. Acta 170 (2010) 27–32.

[16] T.L. Liao, Y.F. Wang, X.B. Zhou, Y. Zhang, X.H. Liu, J. Du, X.J. Li, X.Q. Lu, Detection of DNA damage induced by styrene oxide in ds-DNA layer-by-layer films using adriamycin as electroactive probe, Colloids Surf. B 76 (2010) 334–339.

[17] X.Y. Lin, Y.N. Ni, S. Kokot, An electrochemical DNA-sensor developed with the use of Methylene Blue as a redox indicator for the detection of DNA damage induced by endocrine disrupting compounds. Anal. Chim. Acta 867 (2015) 29-37.

[18] Y.N. Ni, P.P. Wang, H.Y. Song, X.Y. Lin, S. Kokot, Electrochemical detection of benzo (a) pyrene and related DNA damage using DNA/hemin/nafion-graphene biosensor. Anal. Chim. Acta 821 (2014) 34-40.

[19] F. Lauretti, F. Lucas de Melo, F. J. Benati, E. de Mello Volotao, N. Santos, R. E. C. Linhares, C. Nozawa, Use of acridine orange staining for the detection of rotavirus RNA in polyacrylamide gels, J. Virol Methods 114 (2003) 29–35.

[20] E. L. Kostoryz, D. M. Yourtee, Oxidative mutagenesis of doxorubicin-Fe(III) complex, Mutat. Res. 490 (2001) 131–139.

[21] S. Nafisi, A.A. Saboury, N. Keramat, J. F. Neault, H. A. Tajmir-Riahi, Stability and structural features of DNA intercalation with ethidium bromide, acridine orange and methylene blue, J. Mol. Struct. 827 (2007) 35–43.

[22] D. Pastre, O. Pietrement, A. Zozime, E. Le Cam, Study of the DNA/ethidium bromide interactions on mica surface by atomic force microscope: Influence of the surface friction, Biopolymer 77 (2005) 53–62.

[23] M. R. Bugs, M. L. Cornelio, Analysis of the Ethidium Bromide Bound to DNA by Photoacoustic and FTIR Spectroscopy, Photochem. Photobiol. 74 (2001) 512– 520.

[24] V.C. Diculescu, A.M.C. Paquim, A.M.O. Brett, Electrochemical DNA sensors for detection of DNA damage, Sensors 5 (2005) 377-393.

[25] P. O. Vardevanyan, A. P. Antonyan, Investigation of DNA complexes with ligands having different nature. Biolog. J. of Armenia 62 (2010) 50–58 (in Russian).

[26] S. Bi, Ch. Qiao, D. Song, Y. Tian, D. Gao, Y. Sun, H. Zhang, Detection of chemically induced damage in layered DNA films with Co(bpy)3+ by square wave voltammetry, Sensors and Actuators B 119 (2006) 199–208.

[27] Discovery Studio. Accelrys Software Inc, San Diego, CA, (2009). http://www.accelrys.com.

[28] A Politi, S. Durdagi, P. Moutevelis-Minakakis, G. Kokotos, T. Mavromoustakos, Development of accurate binding affinity predictions of novel renin inhibitors through molecular docking studies, J. Mol Graph Model 29 (2010) 425-435.

[29] FA. Momany, RJ. Rone, Validation of the general purpose QUANTA ®3.2/CHARMm® force field, J. Comput. Chem. 13 (1992) 888-900.

[30] D. Van der Spoel, E. Lindahl, B. Hess, G. Groenhof, A. E. Mark, H. J. C. Berendsen, GROMACS: Fast, flexible, and free, J. Comput. Chem. 26 (2005) 1701–1718.

[31] V. Hornak, R. Abel, A. Okur, B. Strockbine, A. Roitberg, C. Simmerling, Comparison of multiple Amber force fields and development of improved protein backbone parameters, Proteins: Struct. Funct. Bioinformat. 65 (2006) 712–725.

[32] L. Rivail, C. Chipot, B. Maigret, I. Bestel, S. Sicsic, M. Tarek, Large-scale molecular dynamics of a G protein-coupled receptor, the human 5-HT_4 serotonin receptor, in a lipid bilayer, J. Mol. Struct. 817 (2007) 19-26.

[33] B. Hess, H. Bekker, H. J. C. Berendsen, J. G. E. M. Fraaije, LINCS: A linear constraint solver for molecular simulations, J. Comput. Chem. 18 (1997) 1463-1472.

[34] T. Darden, D. York, L. Pedersen, Particle mesh Ewald: An N log (N) method for Ewald sums in large systems, J. Chem. Phys. 98 (1993) 10089–10092.

[35] U. Essmann, L. Perera, M. L. Berkowitz, T. Darden, H. Lee, L. G. Pedersen, A smooth particle mesh Ewald method, J. Chem. Phys. 103 (1995) 8577–8593.

[36] H. J. C. Berendsen, J. P. M. Postma, W. F. Van Gunsteren, A. DiNola, J. R. J. Haak, Molecular dynamics with coupling to an external bath, J. Chem. Phys. 81 (1984) 3684–3690.

[37] A. A. Ensafi, M. Jafari-Asl, B. Rezaei, A new strategy for the synthesis of 3-D Pt nanoparticles on reduced graphene oxide through surface functionalization, Application for methanol oxidation and oxygen reduction, Electrochim. Acta 130 (2014) 397–405.

[38] A. A. Ensafi, E. Heydari-Bafrooei, M. Amini, DNA-functionalized biosensor for riboflavin based electrochemical interaction on pretreated pencil graphite electrode, Biosens. Bioelectron. 31 (2012) 376– 381.

[39] H. Guo, X. F. Wang, Q. Y. Qian, F. B. Wang, X. H. Xia, A Green Approach to the Synthesis of Graphene Nanosheets, J. Am. Chem. Soc. 3 (2009) 2653–2659.

[40] L. Chen, Y. Tang, K. Wang, C. Liu, S. Luo, Direct electrodeposition of reduced graphene oxide on glassy carbon electrode and its electrochemical application, Electrochem. Comm. 13 (2011) 133–137.

[41] Y. Jiang, Y. Lu, F. Li, T. Wu, L. Niu, W. Chen. Facile electrochemical codeposition of “clean” graphene–Pd nanocomposite as an anode catalyst for formic acid electrooxidation, Electrochem. Comm. 19 (2012) 21–24

[42] H. L. Guo, X. F. Wang, Q. Y. Qian, F. B. Wan g, X H. Xia, A Green Approach to the Synthesis of Graphene Nanosheets, ACS nano 3 (2009) 2653–2659.

[43] F. Qu, N. Q. Li, Y. Y. Jiang, Electrochemical Studies of CuTMAP Interaction with DNA and Determination of DNA, Talanta 45 (1998) 787–793.

[44] F. Wang, Y. Xu, J. Zhao, S. Hu, Electrochemical oxidation of morin and interaction with DNA, Bioelectrochemistry 7 (2007) 356–362.

[45] X. Tian, Y. Song, H. Dong, B. Ye, Interaction of anticancer herbal drug berberine with DNA immobilized on the glassy carbon electrode, Bioelectrochemistry 73 (2008) 18–22.

[46] A. J. Bard, L. R. Faulkner, Electrochemical Methods and Application, John Wiley and sons, New York, (2001).

Table 1
EDS results from GO and rGO.

Element	line		Intensity (c/s)		Atomic %		Conc.		Unit
	GO	rGO	GO	rGO	GO	rGO	GO	rGO	
C	K_a	K_a	66.81	80.04	61.59	71.49	52.63	63.62	Wt.%
O	K_a	K_a	18.79	12.50	38.41	28.51	47.37	36.38	Wt.%
Total					100.0	100.0	100.0	100.0	Wt.%

Table 2
Linear regression equation of the calibration curves of AO in the presence of different concentrations of kaempferol, fisetin and myricetin.

Antioxidant	**Kaempferol**	**Fisetin**	**Myricetin**
Concentration (nmol L^{-1})			
---	Is=4.51(±2.20)+1.83C(± 0.21)	Is=4.51(±2.20)+1.83C(±0.21)	Is=4.51(±2.20)+1.83C(±0.21)
0.01	Is=0.76(±0.20)+0.18C(±0.02)	Is=0.57(±0.10)+0.17C(±0.01)	Is=0.44 (±0.64)+0.20C(±0.02)
1.00	Is=0.88(±0.16)+0.16C(±0.02)	Is=0.77(±0.31)+0.17C(±0.02)	Is=0.46(±0.17)+0.25C(±0.01)
100	Is=1.18(±0.45)+0.16C(±0.05)	Is=2.56(±0.50)+0.16C(±0.05)	Is=0.36(±0.41)+0.25C(±0.02)

Table 3

The Gold score fitness of the best conformers of kaempferol, fisetin and myricetin docked into the three binding sites of average structures of DNA duplex at different time intervals.

Antioxidant		**Kaempferol**	**Fisetin**	**Myricetin**
Time interval				
1-2 ns (binding site b)		44.52	42.90	44/23
2-3 ns (no binding site)		-	-	-
3-4 ns (binding site a)		45/13	47.99	44.45
4-5 ns	**binding sites a**	36.65	48.03	43.40
	binding sites c	45.99	30.81	41.05

Legends for the figures:

Fig. 1: (A): Cyclic voltammograms of the electroreduction exfoliate graphene oxide in borate buffer (pH 9.0) at a scan rate of 25 mV s^{-1}. (B): Cyclic voltammograms of $Fe(CN)_6^{3-/4-}$ solution (5.0 mmol L^{-1}) containing KNO_3 (0.1 mol L^{-1}) at 1): SPCE, 2): Treated-SPCE and 3): SPGE, with a scan rate of 50 mV s^{-1}. (C): Nyquist plots of $Fe(CN)_6^{3-/4-}$ solution at 1): SPCE, 2): Treated-SPCE and 3): SPGE.

Fig. 2: (A): FTIR and (B): Raman spectra of EGO and rGO samples, respectively. (C): FE-SEM images of SPCE, and (D): FE-SEM images of SPGE. Energy dispersive X-ray spectroscopy results of (E): EGO and (F): rGO.

Fig. 3: Effect of (A): The adsorption potential applied during the DNA immobilization step at SPGE on the guanine and adenine signals; (B): Effect of ds-DNA concentration for immobilization of the ds-DNA at SPGE on the guanine and adenine signals; (C): Accumulation time for immobilization of the ds-DNA at SPGE on the guanine and adenine signals; and (D): Influence of incubation time for AO at the DNA-biosensor. Conditions: scanning potential between +0.40 and +1.40 V, a pulse amplitude of 0.06 V, a modulation time of 0.04 s and a step potential of 0.01 V in acetate buffer solution (pH 4.8).

Fig. 4: A): Differential pulse voltammograms for the interaction of AO at the ds-DNA-modified SPGE; The oxidation signals of guanine and adenine after their interaction with 0.0, 1.0, 5.0, 10.0, 15.0, 50.0, 200.0 and 500.0 pmol L^{-1} AO (from up to down); Differential pulse voltammograms for the interaction of AO at the ds-DNA-modified SPGE; The oxidation signals of guanine and adenine after their interaction with 0.0, 1.0, 5.0, 10.0, 15.0, 50.0, 200.0 and 500.0 pmol L^{-1} AO (from up to down) in the presence of 0.10 µmol L^{-1} B): Fisetin, C): Kaempferol, and D): Myricetin. Conditions as in Fig. 3.

Fig. 5: Fluorescence spectra of AO with different concentrations as 5.0, 10.0, 15.0, 20.0, 25.0, 30.0, 35.0 and 40.0 nmol L^{-1} (from down to up) in the presence of 20.0 mg L^{-1} ds-DNA and 0.010 nmol L^{-1} of A): fisetin, B): kaempferol and D): myricetin.

Fig. 6: Fluorescence spectra of 25 nmol L^{-1} AO before and after in the presence of 1.0 µmol L^{-1}, A): kaempferol, B): fisetin, and C): myricetine.

Fig. 7: The best conformer of fisetin docked in the three binding sites of DNA duplex at different time intervals by the use of GOLD program results in hydrogen bonds and π-σ interactions. H-bonds are marked by dotted-green lines and π interactions are shown in orange lines.

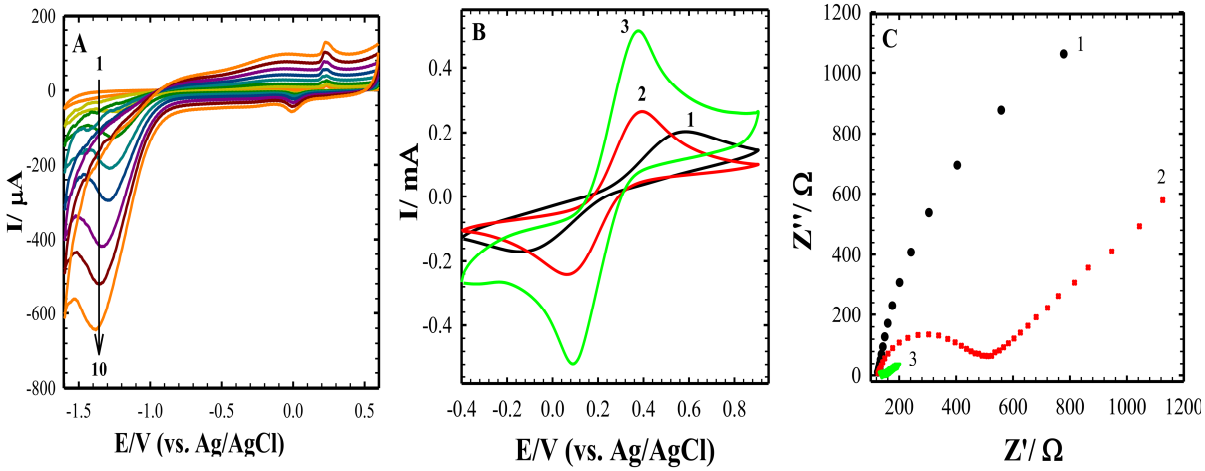

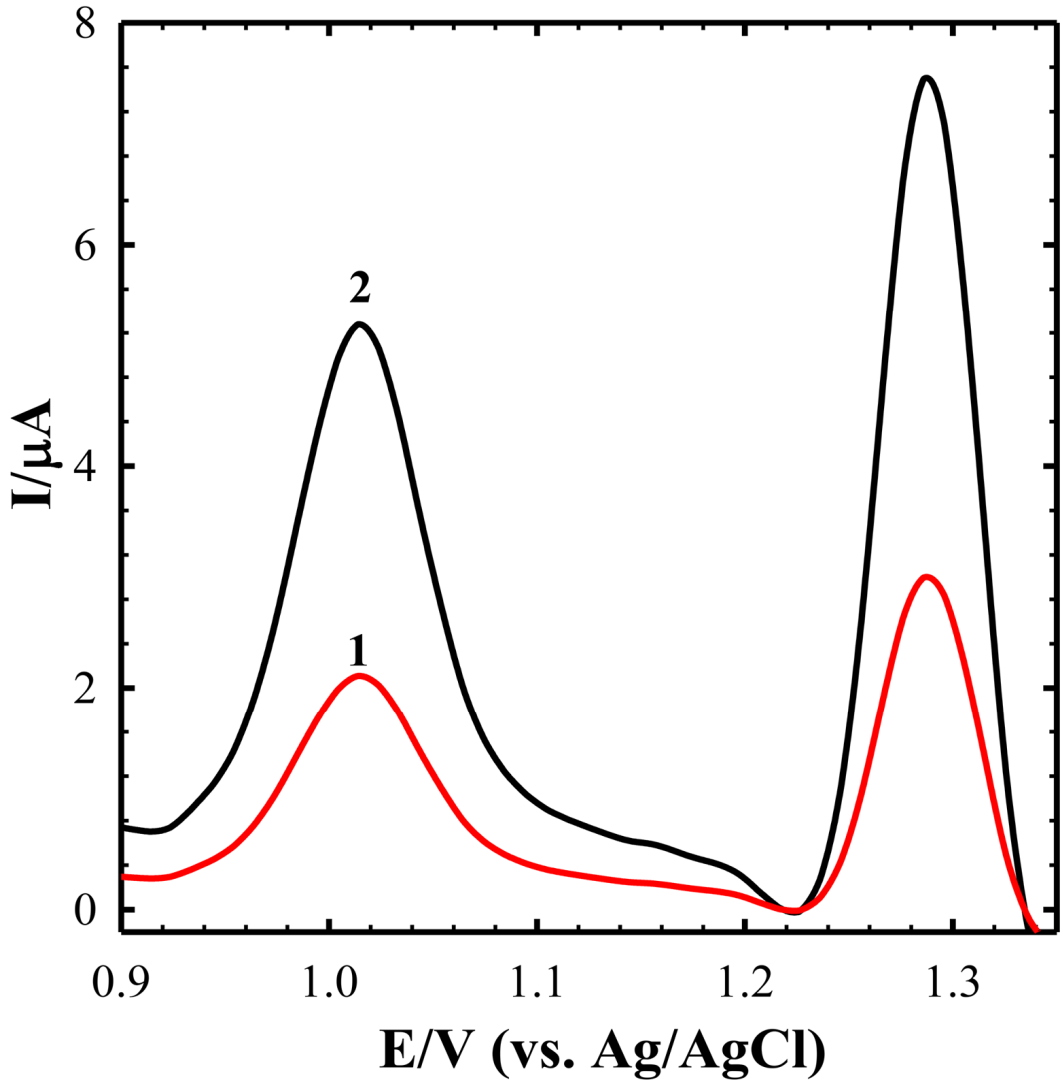

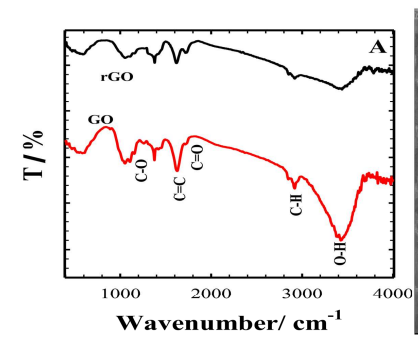

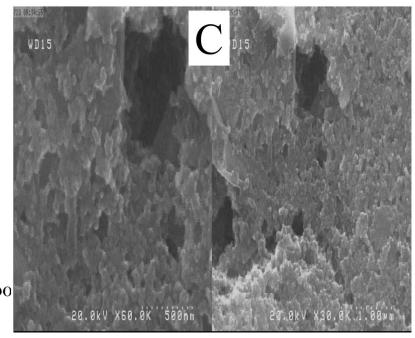

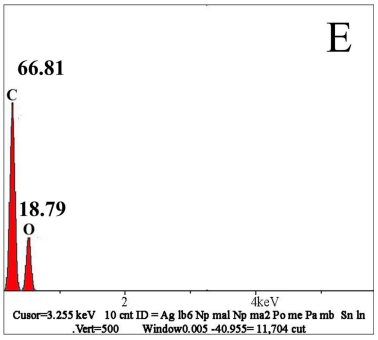

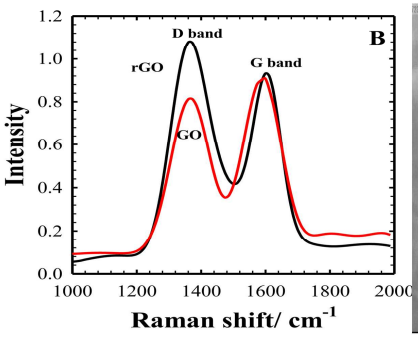

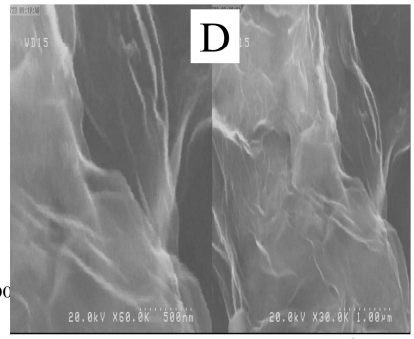

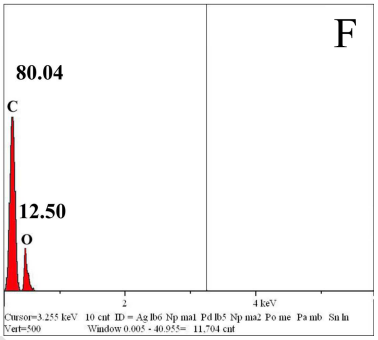

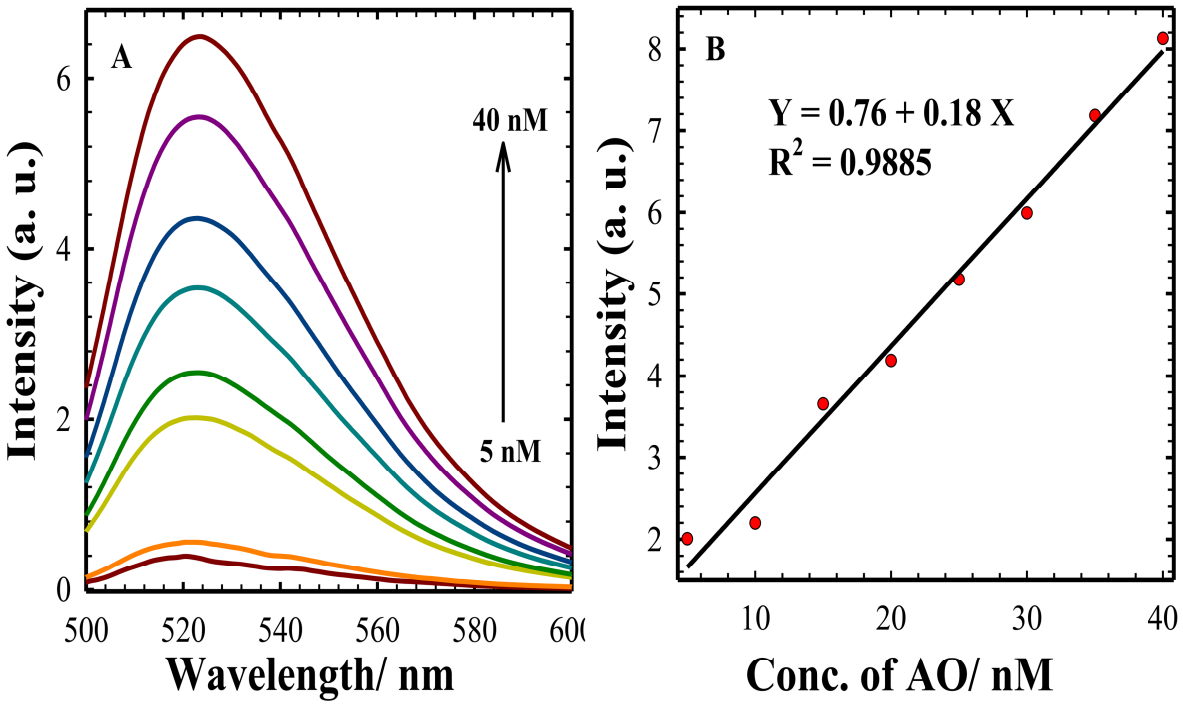

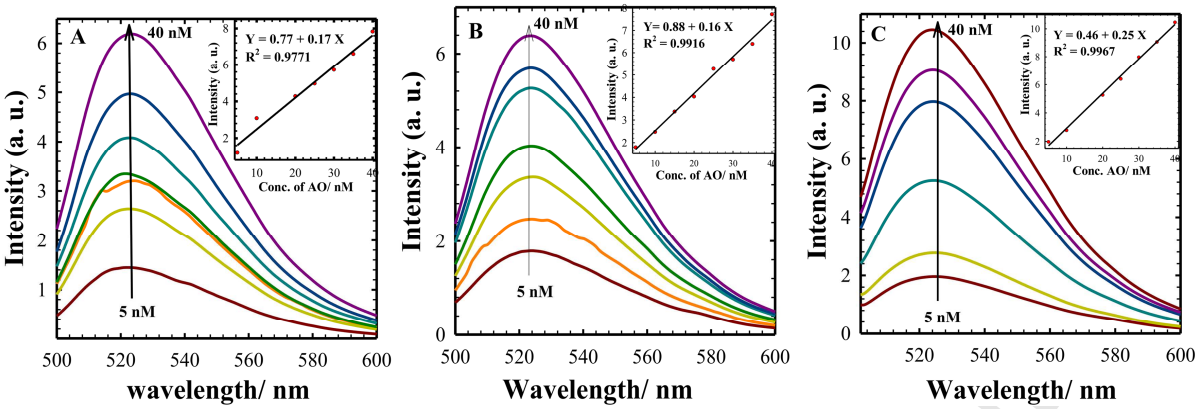

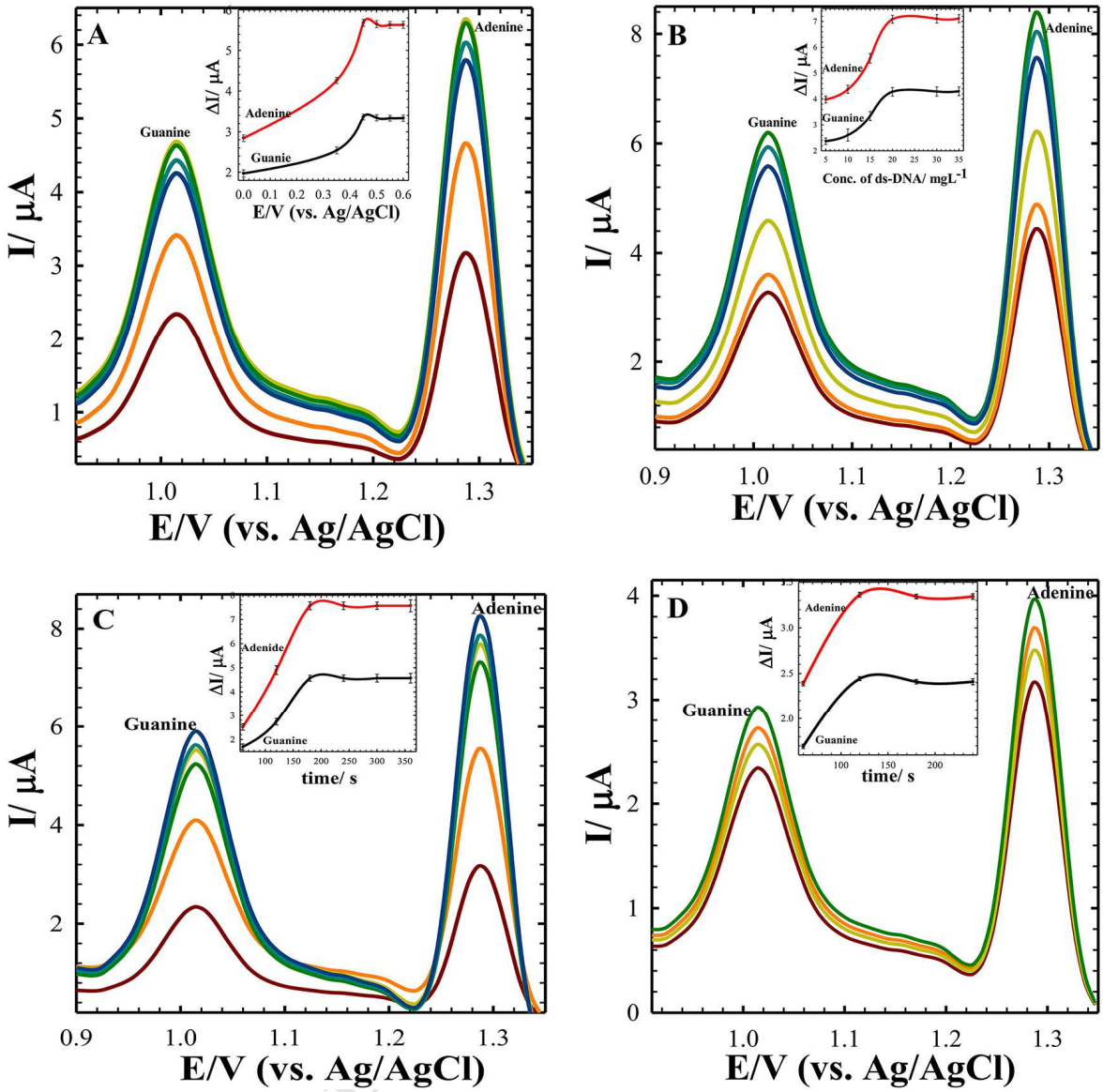
A
Guanine
Adenine
I/ µA
E/V (vs. Ag/AgCl)
ΔI/ µA
Adenine
Guanie
E/V (vs. Ag/AgCl)
B
Guanine
Adenine
I/ µA
E/V (vs. Ag/AgCl)
ΔI/ µA
Adenine
Guanine
Conc. of ds-DNA/ mgL-1
C
Guanine
Adenine
I/ µA
E/V (vs. Ag/AgCl)
ΔI/ µA
Adenide
Guanine
time/ s
D
Guanine
Adenine
I/ µA
E/V (vs. Ag/AgCl)
ΔI/ µA
Adenine
Guanine
time/ s

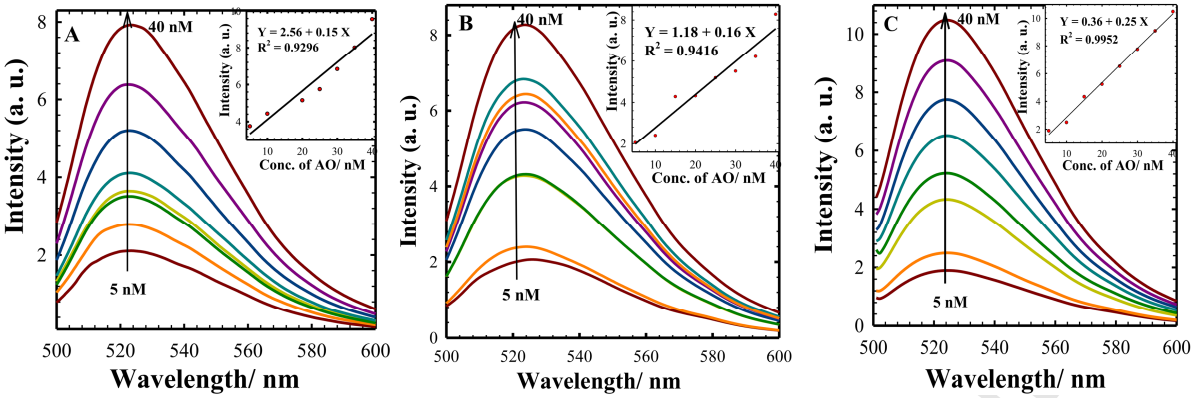

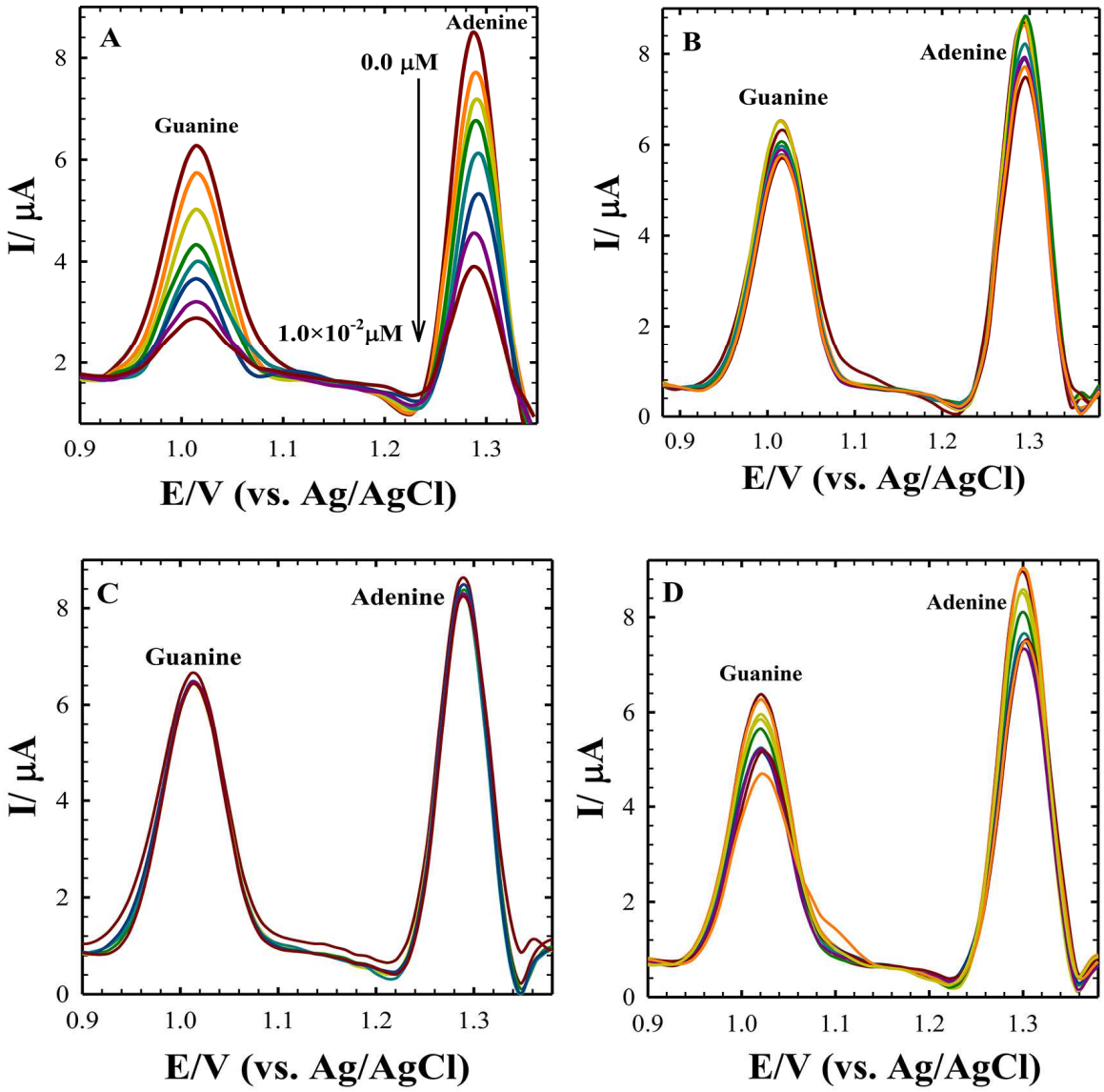
A
Adenine
0.0 μM
Guanine
1.0×10-2μM
I/ μA
E/V (vs. Ag/AgCl)
B
Adenine
Guanine
I/ μA
E/V (vs. Ag/AgCl)
C
Adenine
Guanine
I/ μA
E/V (vs. Ag/AgCl)
D
Adenine
Guanine
I/ μA
E/V (vs. Ag/AgCl)

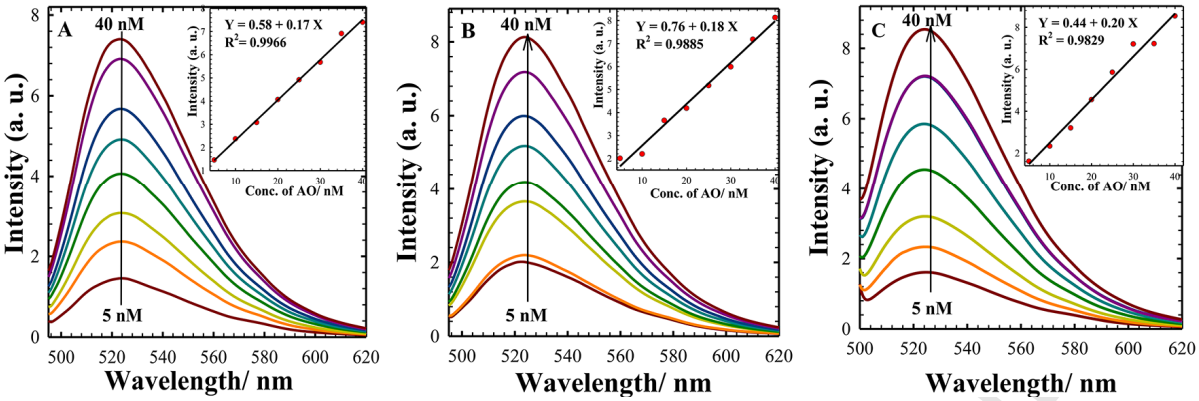

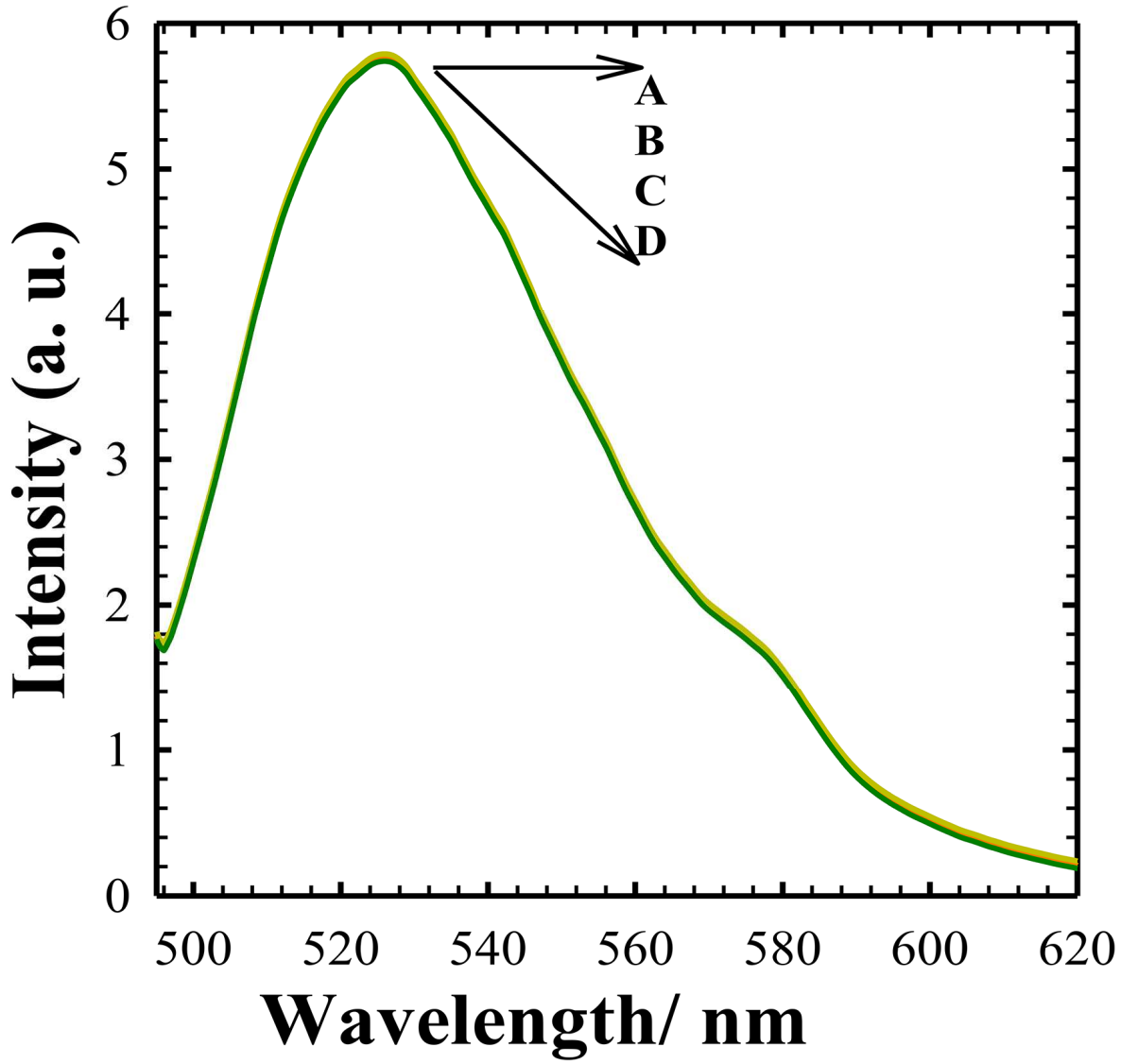

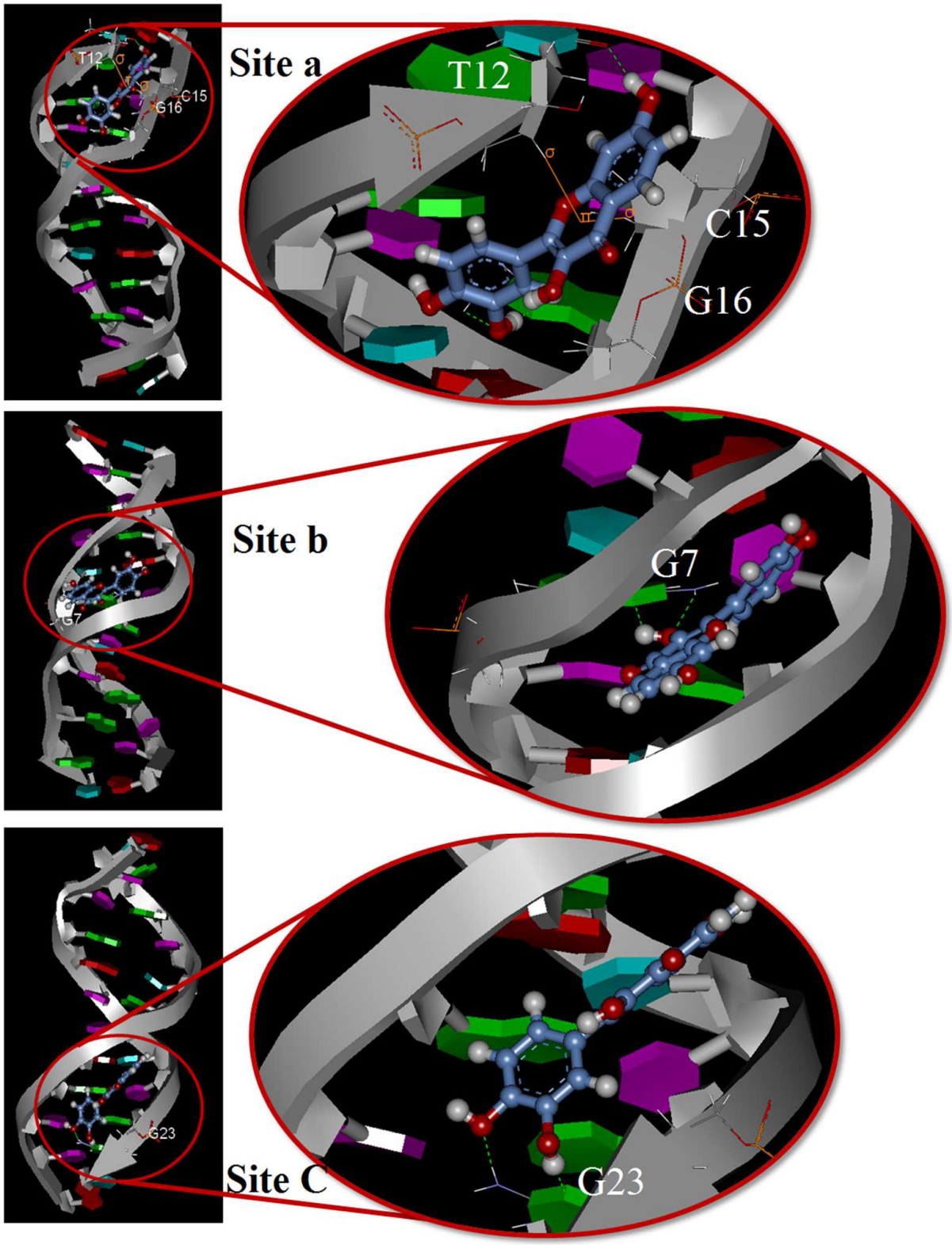
T12
C15
G16
Site a
T12
C15
G16
G7
Site b
G7
G23
Site C
G23

- A simple methodology was used to develop a biosensor to check DNA damage.
- The ability of three flavonols antioxidants to prevent DNA damage were studied.
- Acridine orange was used as a DNA damaging agent.
- Uv-Vis and fluorescence spectroscopy were used to confirm the electrochemical results.

Supplementary materials

Experimental and theoretical investigation effect of flavonols antioxidants on DNA damage

Ali A. Ensafi[*1], E. Heydari-Soureshjani[1], M. Jafari-Asl[1], B. Rezaei[1], Jahan B. Ghasemi[2], Elham Aghaee[2]

(1) Department of Analytical Chemistry, Faculty of Chemistry, Isfahan University of Technology, Isfahan 84156–83111, Iran

(2) Drug Design in Silico Lab., Chemistry Faculty, K N Toosi University of Technology, Tehran, Iran

To camper SPCE and SPGE as a substrate for immobilizing of the DNA, differential pulse voltammograms of ds-DNA at the surfaces of these two substrate were recorded. For this purpose, the ds-DNA was immobilized on the surface of SPCE and SPGE by applying a potential at +0.45 V for 180 s from a stirred (constant rate) solution containing 20.0 mg L^{-1} ds-DNA in an acetate buffer containing 0.02 mol L^{-1} NaCl (pH 4.8). The scanning potential was changed between +0.40 and +1.40 V with a pulse amplitude of 0.06 V, a modulation time of 0.04 s and a step potential of 0.01 V. The results are shown in Fig. S-1. The results show that the oxidation peaks current of guanine and adenine on the DNA/SPGE is higher than the DNA/SPCE, because the surface area of SPGE in higher than SPCE, and therefore, more DNA can be assembled on the surface of the electrode.

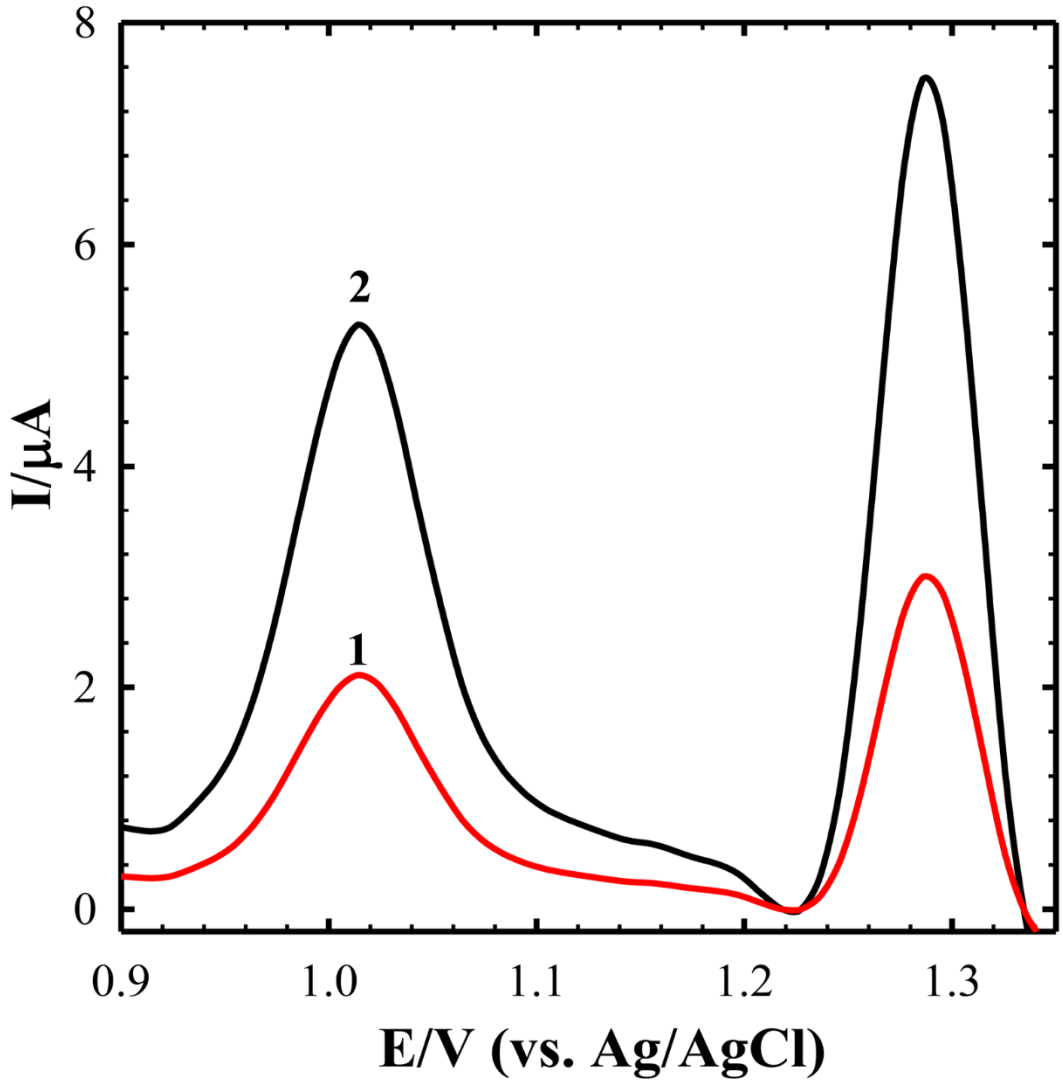

Fig. S-1: Differential pulse voltammograms of ds-DNA at 1): SPCE and 2): SPGE. Conditions: The ds-DNA was immobilized on a SPCE and SPGE surface by applying a potential at +0.45 V for 180 s from a stirred (constant rate) solution containing 20.0 mg L^{-1} ds-DNA. Conditions: scanning potential between +0.40 and +1.40 V, pulse amplitude of 0.06 V, modulation time of 0.04 s and step potential of 0.01 V in the acetate buffer solution containing 0.02 mol L^{-1} NaCl (pH 4.8).

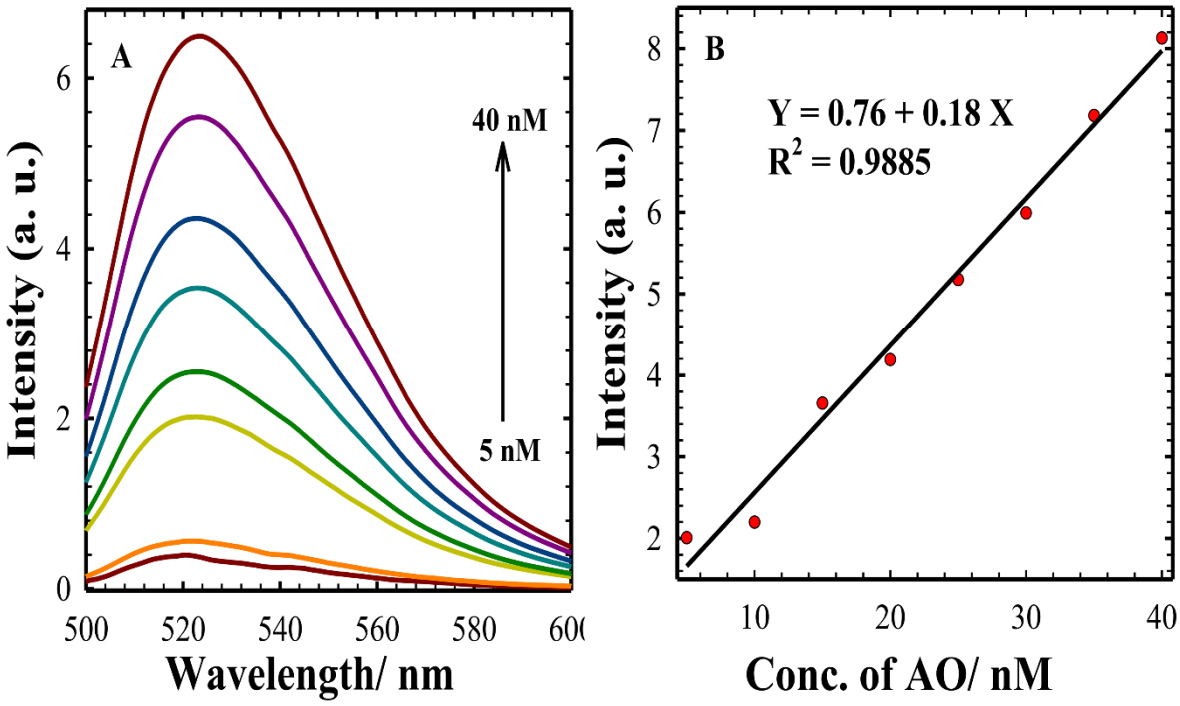

Fig. S-2: Fluorescence spectra (A) and linear variations in the fluorescence intensity of AO (B) with increasing its concentration as 5.0, 10.0, 15.0, 20.0, 25.0, 30.0, 35.0 and 40.0 nmol L^{-1} (from down to up) in the presence of ds-DNA (20.0 mg L^{-1}).

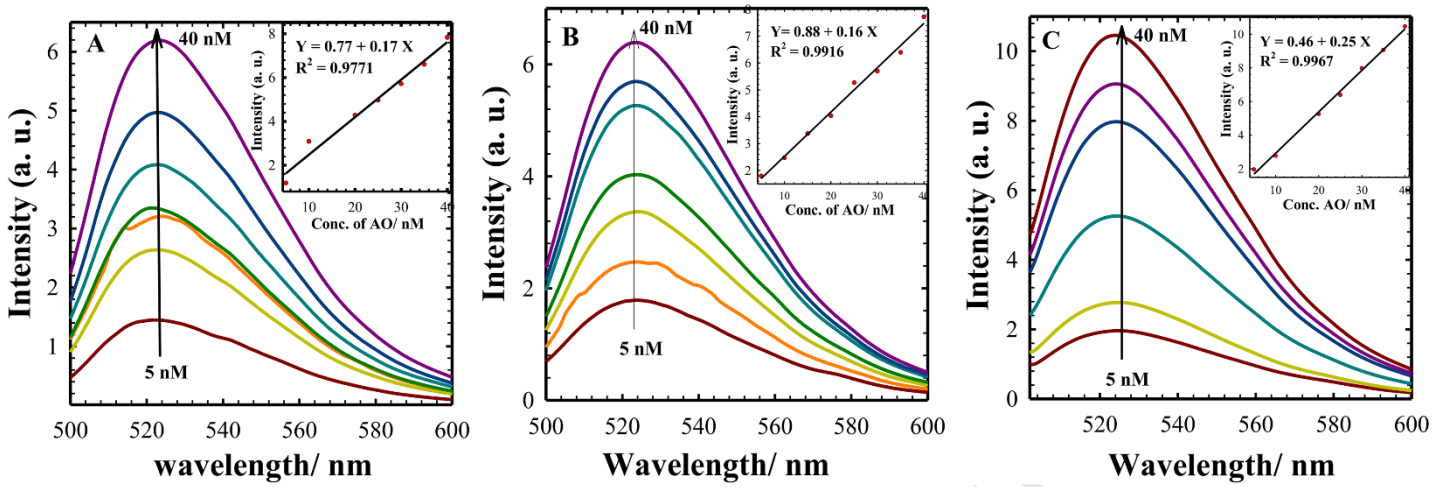

Fig. S-3: Fluorescence spectra of different concentration of AO as 5.0, 10.0, 15.0, 20.0, 25.0, 30.0, 35.0 and 40.0 nmol L^{-1} (from down to up) in the presence of 20.0 mg L^{-1} ds-DNA and 1.0 nmol L^{-1} of A): fisetin, B): kaempferol and D): myricetin. Inset: Linear variations in the fluorescence intensity of AO with its concentration.

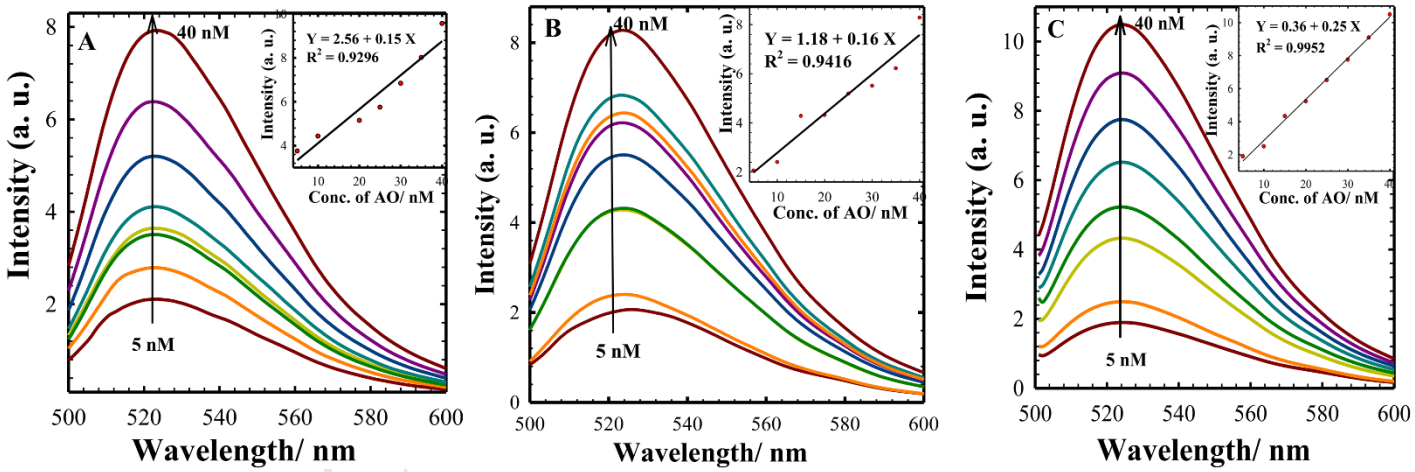

Fig. S-4: Fluorescence spectra of different concentration of AO as 5.0, 10.0, 15.0, 20.0, 25.0, 30.0, 35.0 and 40.0 nmol L^{-1} (from down to up) in the presence of 20.0 mg L^{-1} ds-DNA and 100 nmol L^{-1} of A): fisetin, B): kaempferol and D): myricetin. Inset: Linear variations in the fluorescence intensity of AO with its concentration.